

Article

Camostat Does Not Inhibit the Proteolytic Activity of Neutrophil Serine Proteases

Akmaral Assylbekova¹, Anuar Zhanapiya¹, Renata Grzywa², Marcin Sienczyk², Christian Schönbach¹ 
and Timo Burster^{1,*} 

¹ Department of Biology, School of Sciences and Humanities, Nazarbayev University, Kabanbay Batyr Ave. 53, Nur-Sultan 010000, Kazakhstan; akmaral.assylbekova@nu.edu.kz (A.A.); anuar.zhanapiya@nu.edu.kz (A.Z.); christian.schoenbach@nu.edu.kz (C.S.)

² Division of Medicinal Chemistry and Microbiology, Faculty of Chemistry, Wrocław University of Science and Technology, Wybrzeże Wyspiańskiego 27, 50-370 Wrocław, Poland; renata.grzywa@pwr.edu.pl (R.G.); marcin.sienczyk@pwr.wroc.pl (M.S.)

* Correspondence: timo.burster@nu.edu.kz

Abstract: Coronavirus disease 2019 (COVID-19) can lead to multi-organ failure influenced by comorbidities and age. Binding of the severe acute respiratory syndrome coronavirus 2 spike protein (SARS-CoV-2 S protein) to angiotensin-converting enzyme 2 (ACE2), along with proteolytic digestion of the S protein by furin and transmembrane protease serine subtype 2 (TMPRSS2), provokes internalization of SARS-CoV-2 into the host cell. Productive infection occurs through viral replication in the cytosol and cell-to-cell transmission. The catalytic activity of TMPRSS2 can be blocked by the trypsin-like serine protease inhibitor camostat, which impairs infection by SARS-CoV-2. At the site of infection, immune cells, such as neutrophils, infiltrate and become activated, releasing neutrophil serine proteases (NSPs), including cathepsin G (CatG), neutrophil elastase (NE), and proteinase 3 (PR3), which promote the mounting of a robust immune response. However, NSPs might be involved in infection and the severe outcome of COVID-19 since the uncontrolled proteolytic activity is responsible for many complications, including autoimmunity, chronic inflammatory disorders, cardiovascular diseases, and thrombosis. Here, we demonstrate that camostat does not inhibit the catalytic activity of CatG, NE, and PR3, indicating the need for additional selective serine protease inhibitors to reduce the risk of developing severe COVID-19.

Keywords: serine proteases; cathepsin G; neutrophil elastase; proteinase 3; camostat; SARS-CoV-2; COVID-19



Citation: Assylbekova, A.; Zhanapiya, A.; Grzywa, R.; Sienczyk, M.; Schönbach, C.; Burster, T. Camostat Does Not Inhibit the Proteolytic Activity of Neutrophil Serine Proteases. *Pharmaceuticals* **2022**, *15*, 500. <https://doi.org/10.3390/ph15050500>

Academic Editors: Jean Leandro dos Santos and Chung Man Chin

Received: 15 March 2022

Accepted: 15 April 2022

Published: 20 April 2022

Publisher's Note: MDPI stays neutral with regard to jurisdictional claims in published maps and institutional affiliations.



Copyright: © 2022 by the authors. Licensee MDPI, Basel, Switzerland. This article is an open access article distributed under the terms and conditions of the Creative Commons Attribution (CC BY) license (<https://creativecommons.org/licenses/by/4.0/>).

1. Introduction

Processing of the severe acute respiratory syndrome coronavirus 2 spike protein (SARS-CoV-2 S protein) is a prerequisite for infection of the target cell and influences the outcome of coronavirus disease 2019 (COVID-19). More precisely, proteolytic cleavage of the S protein by the cell surface serine proteases furin and the transmembrane protease serine subtype 2 (TMPRSS2) is required to fuse the S protein with the target cell membrane. This mechanism is performed in a two-step sequential hydrolysis. The priming cleavage between the S1/S2 interface by furin is followed by an activating cleavage by TMPRSS2 at the S2' site [1–5]. Hydrolysis of the SARS-CoV-2 S protein by TMPRSS2 remains an essential step in the process of viral entry into the host cell. Indeed, camostat mesylate (camostat), a clinically proven trypsin-like serine protease inhibitor for treating chronic pancreatitis and postoperative reflux esophagitis, inhibits TMPRSS2 and prevents SARS-CoV-2 infection of target cells. As a result, camostat has been repurposed in clinical trials for the potential therapeutic management of COVID-19 [6,7].

In general, the activity of proteases is precisely regulated to avoid harmful degradation of structural or functional proteins by endogenous natural inhibitors, so-called serine

protease inhibitors (serpins) [8,9]. The majority of proteases located at the site of infection originate from activated neutrophils. These neutrophils secrete NSPs from granules including cathepsin G (CatG), neutrophil elastase (NE), protease 3 (PR3), and neutrophil serine protease 4 (NSP4) [10]. After an immune response, proteases need to be regulated to a steady-state; however, deregulation of NSPs and their endogenous serine protease inhibitors can result in chronic inflammatory disorders. In particular, the uncontrolled proteolytic activity of, for instance, CatG is involved in autoimmunity, chronic inflammatory diseases, cardiovascular diseases, and thrombosis [11]. Furthermore, it was demonstrated that the abundance of CD15⁺ neutrophils and CatG transcripts was elevated in COVID-19 patients [12], increased concentrations of NE and CatG were determined in nasopharyngeal swabs of patients with SARS-CoV-2 [13], and levels of CatG in plasma were increasingly higher starting with the control group to moderate, severe, and critical COVID-19 conditions [14]. In addition, CatG might also be responsible for priming the S protein at the S1/S2 interface (polybasic sequence) of the proteolytic sensitive activation loop of the SARS-CoV-2 Omicron variant [15]. These observations indicate the relevance of CatG in COVID-19.

Proteases are characterized depending on the catalytic mechanism to hydrolyze the sessile peptide bonds within a protein. Serine proteases, one of the largest groups, encompass the S1 family, which is further divided into three subfamilies: (i) trypsin-like serine proteases with a preference for basic amino acids, for instance, TMPRSS2, (ii) chymotrypsin-like serine proteases which favor bulky hydrophobic amino acids, and (iii) elastase-like serine proteases with small aliphatic amino acids as preferred amino acid residues in P1 which is the position between two amino acids of the sessile peptide bond towards the N terminal end. While CatG possesses both chymotrypsin-like and trypsin-like serine protease capability, NE, as well as PR3, belong to the elastase-like serine proteases [8]. Several inhibitors are available and classified into two major groups (peptide- or protein-based and non-peptide inhibitors) to antagonize the proteolytic activity of serine proteases. Of these, alpha-1 antitrypsin, aprotinin, and chymostatin belong to the first group, and diphenyl esters of phosphonates, β -keto-phosphonic acid, phenol ester, heparin, and boswellic acid derivatives are categorized to the second group [16]. For instance, sunflower-derived serine protease inhibitors (SFTI) and their derivatives are selective CatG inhibitors based on a 14 amino acid cyclic peptide [17,18]. Peptidyl diphenyl phosphonates are an additional class of serine protease inhibitors, including Suc-Val-Pro-Phe^P(OPh)₂, which blocks the proteolytic activity of CatG [19]. Furthermore, sivelestat, which was originally postulated as a selective NE inhibitor [20] to treat acute respiratory distress syndrome [21], also inhibits PR3 [22].

Whether camostat inhibits neutrophil serine proteases (NSPs) is not clear. Thus, we investigated the potential inhibition of CatG, NE, and PR3 by camostat.

2. Results and Discussion

2.1. Activity-Based Protein Profiling of Cathepsin G (CatG) in the Presence of Camostat

Purified CatG was preincubated with different concentrations of camostat and followed by adding the FAM-P1,5D-Suc-Val-Pro-Phe^P(OPh)₂ (MARS116-FAM) activity-based probe (ABP), which is a directly 5(6)-carboxyfluorescein (FAM) conjugated peptidyl diphenyl phosphonate, to analyze whether camostat (Figure 1A) inhibits the proteolytic activity of CatG [23]. Since the phosphorus atom of the MARS116-FAM phosphonate warhead is targeted by a nucleophilic attack of the oxygen atom of CatG's catalytic serine residue, the phosphonate group binds covalently to the serine side chain [24]. Thus, MARS-116-FAM can be used to detect CatG activity in an SDS-PAGE-based assay [24]. As demonstrated in Figure 1B, camostat did not inhibit the catalytic activity of CatG determined by activity-based protein profiling, in contrast to Suc-Val-Pro-Phe^P(OPh)₂ (SucVPPF) or the CatG inhibitor (CatGinh), which blocked the proteolytic activity of CatG at a concentration of 10 μ M.

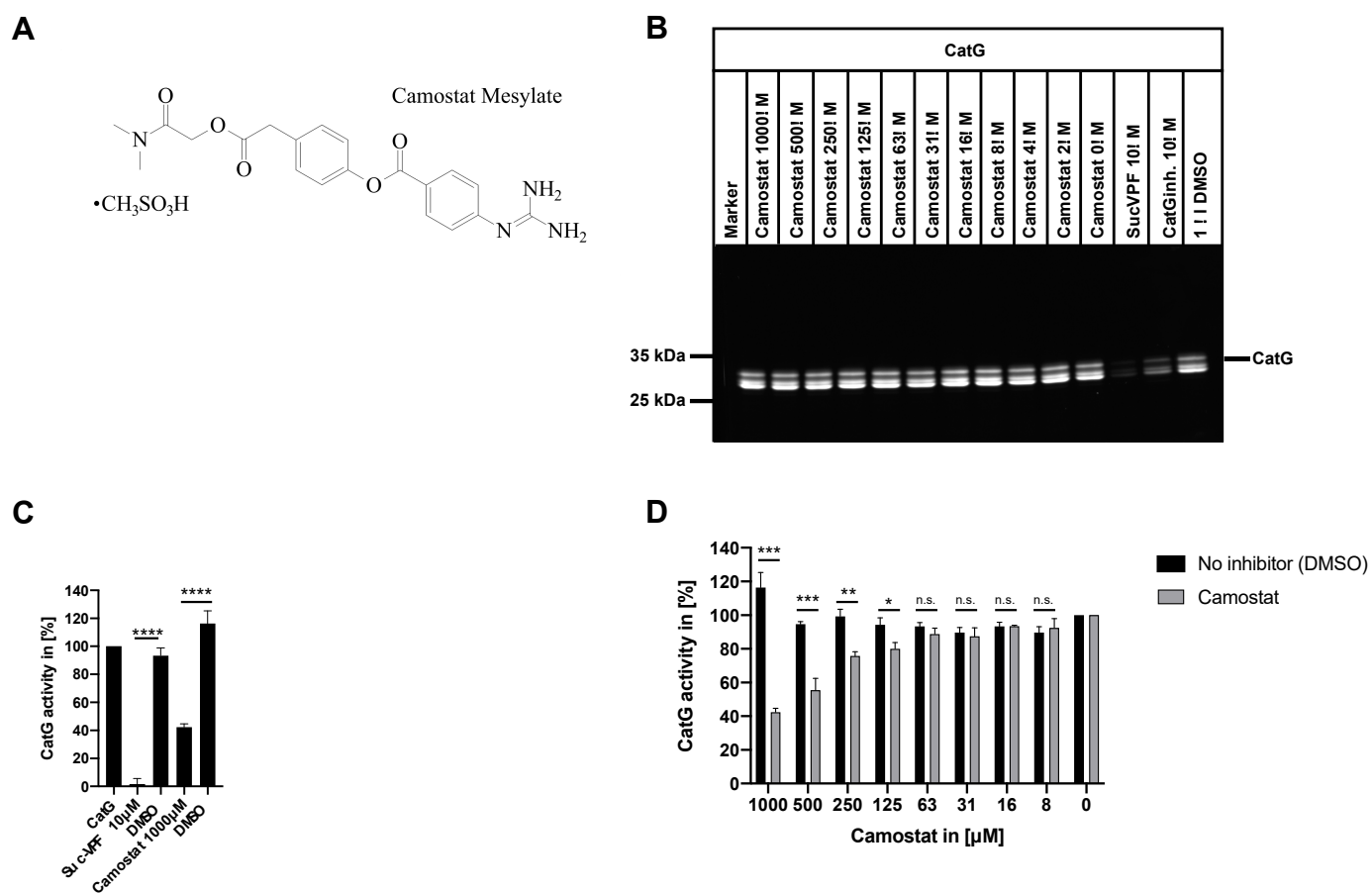


Figure 1. Analysis of the inhibition capacity of camostat towards CatG. (A) The chemical structure of the trypsin-like serine protease inhibitor camostat. (B) Activity-based protein profiling of CatG by using MARS116-FAM with different concentrations of camostat, Suc-Val-Pro-Phe^P(OPh)₂ (SucVPF), or the CatG inhibitor (CatGinh) was performed. DMSO was used as a solvent control. One out of three ($n = 3$) independent experiments is shown. (C) CatG activity was analyzed by using the colorimetric substrate 4-(((S)-3-methyl-1-((S)-2-(((S)-1-((4-nitrophenyl)amino)-1-oxo-3-phenyl-propan-2-yl)-carbamoyl)pyrrolidin-1-yl)-1-oxobutan-2-yl)-amino)-4-oxobutanoic acid (Suc-VPF-pNA). In order to validate the assay, CatG, CatG with SucVPF, CatG with camostat, or the vehicle control CatG with DMSO (the volume of DMSO for camostat was higher) were incubated prior to adding Suc-VPF-pNA. The substrate turnover of Suc-VPF-pNA was analyzed at 405 nm. (D) CatG was preincubated with different concentrations of camostat or DMSO for 15 min at RT. Afterwards, the colorimetric substrate was added to the assay to lead the enzymatic digest. Three independent experiments are summarized, $n = 3$. $p < 0.05$ (*), $p < 0.01$ (**), $p < 0.001$ (***), $p < 0.0001$ (****), or n.s. = not significant.

The turnover of the colorimetric substrate Suc-VPF-pNA by CatG and camostat was used to support the activity-based protein profiling results. CatG was preincubated at different concentrations of camostat, and the hydrolysis of the substrate by CatG was determined. SucVPF or the CatG inhibitor antagonized the proteolytic activity of CatG at 10 μM in contrast to camostat where high concentrations (500 to 1000 μM) were necessary to reduce CatG-mediated hydrolysis substantially (Figure 1C,D). Taken together, these data indicate that camostat does not mitigate CatG activity at reasonable concentrations.

2.2. Activity-Based Protein Profiling of NE and PR3 in the Presence of Camostat

In the next set of experiments, purified NE or PR3 were preincubated with different concentrations of camostat followed by the addition of a FAM-conjugated activity-based probe VPV-FAM. Camostat did not inhibit both NE and PR3 in contrast to sivelestat (Figure 2).

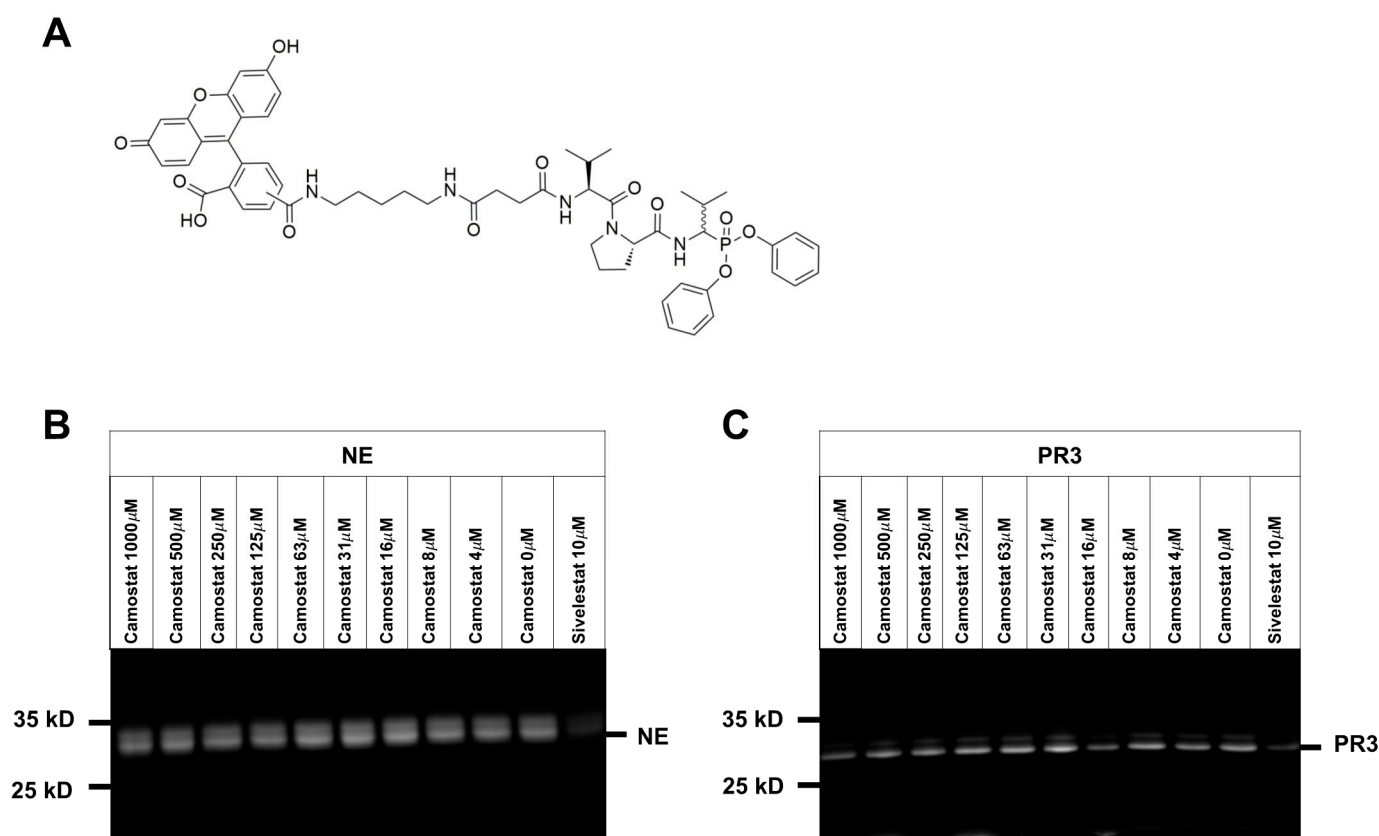


Figure 2. The inhibition capacity of camostat towards NE and PR3 was analyzed by using activity-based protein profiling. (A) Structure of activity-based probe FAM-DAPe-Suc-Val-Pro-Val^P(OPh)₂ (VPV-FAM). (B) Activity-based protein profiling of NE and (C) PR3 by using VPV-FAM with indicated concentrations of camostat was performed. 10 μ M of sivelestat was used as an inhibitor for NE and PR3. One representative gel out of three ($n = 3$) experiments is shown.

Hoffmann et al. found that 10 μ M of camostat reduced infection of primary human lung cells by SARS-CoV-2 [25]. The dosage of 600 mg/day camostat in the SPIKE-1 clinical trial preliminary data resulted in a plasma concentration of $0.2 \mu\text{M} \pm 0.1 \mu\text{M}$ ($87.1 \text{ ng/mL} \pm 29.5 \text{ ng/mL}$, <https://www.covid-19-Camostat-trial.com>, accessed on 17 April 2022). However, in a randomized, double-blinded, placebo-controlled trial with patients receiving 200 mg of camostat three times a day for five days, the clinical outcome of COVID-19 did not improve [26]. Our findings demonstrate that only a very high concentration of 500 to 1000 μ M of camostat considerably reduced the turnover rate of the colorimetric substrate but not directly the proteolytic activity of CatG determined by activity-based protein profiling. The dose of camostat, which is used in clinical trials, is also not sufficient to reduce the proteolytic activity of CatG, NE, and PR3 and might partly explain the outcome of the clinical trial for hospitalized COVID-19 patients.

In order to interpret and correlate the above experimental findings with calculated values of binding free energies and various docking options, a computational method (AutoDock4) was used to predict critical interacting groups between camostat along with NSPs and TMRSS2. Based on this method, the binding free energy of the inhibitor to the catalytic center of the protease can be calculated [27]. The free binding energy for camostat, the camostat inactive metabolite 4-guanidinobenzoic acid (GBA), and CatG inhibitor in complex to CatG (Protein Data Bank ID, PDB ID: 1CGH) was evaluated. As a result, the molecular docking calculation estimated the following values for camostat-CatG -6.52 kcal/mol , GBA-CatG -4.90 kcal/mol , and CatG inhibitor-CatG -9.65 kcal/mol (Figure 3A and Supplementary Tables S1 and S2). Furthermore, the redocked binding energy of SucVPF to CatG corresponded to -8.75 kcal/mol . Notably, the predicted

inhibitor-binding pose of camostat-TMPRSS2 (-8.69 kcal/mol) was supported by GBA-TMPRSS2 (-7.31 kcal/mol) for which X-ray crystallography data are available (7MEQ) [28] (Figure 3B). The camostat's guanidinium group formed a salt bridge to the TMPRSS2 binding pocket D435. Camostat is further stabilized within the hydrophobic patch forming a hydrophobic interaction with V280. Seven hydrogen bonds are determined in the camostat-TMPRSS2 complex [29].

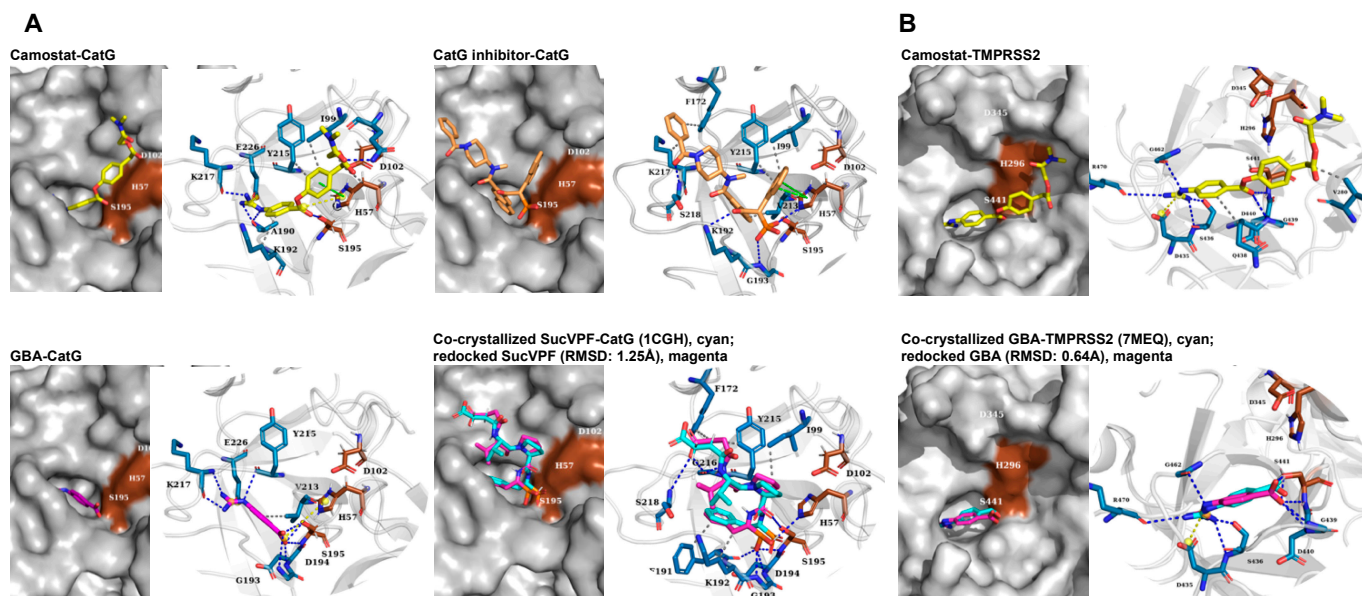


Figure 3. Binding processes of serine protease inhibitors to CatG and TMPRSS2 by using AutoDock4. (A) The catalytic center containing the catalytic triad is tinted brown within the surface model of CatG (grey). Interaction of camostat (yellow), GBA (pink), CatG inhibitor (orange), and SucVPF (green) with CatG. Redocking the co-crystallized SucVPF-CatG (1CGH) complex and SucVPF was performed to validate the docking protocol. (B) Prediction of TMPRSS2 complexed with camostat. Co-crystallized GBA-TMPRSS2 (7MEQ) and redocking with GBA were attributed for validation. The crystal structures of the complexes were analyzed using the protein-ligand interaction profiler (PLIP). The dashed lines correspond to the molecular interactions formed between the inhibitor and the indicated amino acids of CatG or TMPRSS2. Dashed lines in blue, hydrogen bonds; grey, hydrophobic; yellow, salt bridges; green, pi-stacking interactions.

Camostat and sivelestat were estimated for their binding free energies to NE and PR3. The binding simulation of camostat-NE was equivalent to -6.35 kcal/mol and camostat-PR3 -6.19 kcal/mol (Figures 4 and 5, and Supplementary Table S3). Sivelestat, which was used as a control inhibitor, exhibited free binding energy to NE of -7.03 kcal/mol and in the case of PR3 -6.50 kcal/mol (Supplementary Table S3). These indicate a lower affinity of camostat to NE and PR3 in contrast to sivelestat. Additionally, camostat topologically points out of the catalytic center of both NE and PR3 (Figures 4A and 5A), which further explains a non-inhibitory capacity of camostat towards NE and PR3.

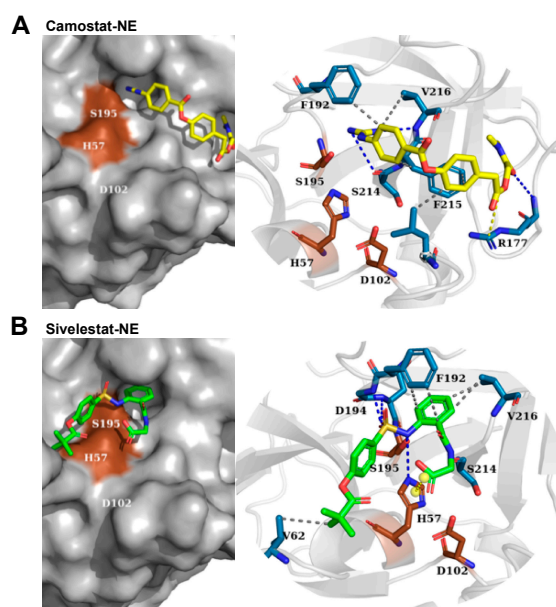


Figure 4. Binding poses of camostat and sivelestat at the catalytic center of NE. Camostat (yellow) and sivelestat (green) were simulated for binding to the catalytic center of NE (1B0F). **(A)** Predicted amino acid residues forming three hydrogen bonds (R177, S214, and V216), three hydrophobic (F192, F215, and V216), and one salt bridge (R177) between camostat and NE. **(B)** sivelestat possesses six hydrogen bonds including H57, G193, D194, S195, and S214, five hydrophobic including V62, F192, and V216, and one salt bridge (H57) with NE. The catalytic triad (brown) within the surface model of NE (grey) and blue dashed lines refer to hydrogen bonds. Hydrophobic interactions and salt bridges are represented by grey- and yellow dashed lines, respectively.

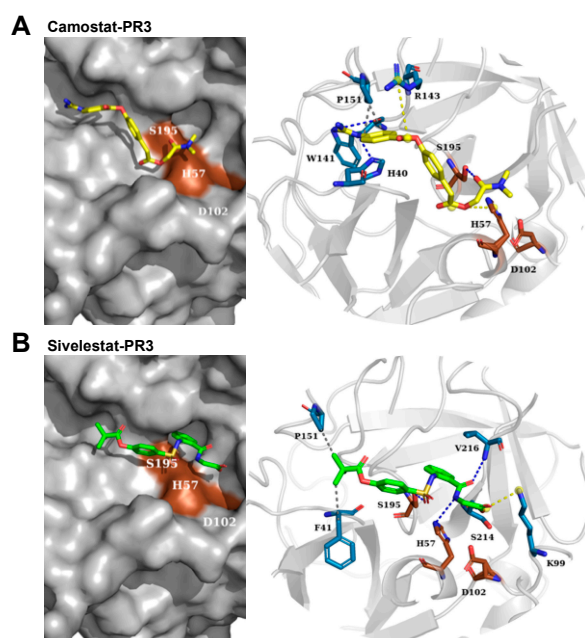


Figure 5. A molecular docking approach was used to determine the binding affinity of camostat and sivelestat to PR3. **(A)** The predicted poses for camostat (yellow) to PR3 (1FUJ) exhibited three hydrogen bonds (H40, W141, and S195), one hydrophobic (P151), and two salt bridges (H57 and R143). **(B)** The ligand-binding affinity prediction of sivelestat (green) results in four hydrogen bonds to PR3 (H57, S195, S214, and V216), two hydrophobic (F41 and P161), and one salt bridge (K99). The catalytic triad (brown), the surface model of NE (grey), blue dashed lines refer to hydrogen bonds, hydrophobic interactions (grey dashed lines), and salt bridges (yellow dashed lines).

While each analyzed inhibitor formed hydrogen bonds with the active-site serine residue (S195) of CatG, the number and intermolecular forces of neighboring residues also change the binding energy and influence the inhibition capacity. For example, the hydrogen bonding of SucVPF and CatG inhibitor with H57, K192, and S218 of CatG, absent in both camostat and GBA, might contribute to the lower predicted free binding energy (Figure 3A and Supplementary Table S2). In contrast, the redocking of GBA to TMPRSS2 (7MEQ) and using the docking approach for camostat to TMPRSS2 showed similar hydrogen bonds and salt bridges within the catalytic center (S436, G439, D440, S441, G462, R470, and D435). The estimated free binding energy was -7.31 kcal/mol for GBA-TMPRSS2 and -8.69 kcal/mol for camostat-TMPRSS2, which are comparable values determined for CatG in the presence of CatG inhibitor or SucVPF (Figure 3 and Supplementary Table S2). The inhibition constant (K_i) was predicted for camostat-TMPRSS2 versus camostat-CatG and was in the order of nanomoles only for camostat-TMPRSS2 (424.27 nM) in contrast to camostat-CatG (16.67 μ M) (Supplementary Table S2). In summary, the differences in the estimated free binding energy of the camostat-CatG complex compared to SucVPF and CatGinh explain that camostat does not inhibit the proteolytic activity of CatG in the activity-based protein profiling experiment (Figure 1B). A similar rationale applies to the non-inhibition of NE and PR3 by camostat (camostat-NE, -6.35 kcal/mol and 21.97 μ M and camostat-PR3, -6.19 kcal/mol and 29.17 μ M, Figures 4 and 5 as well as Supplementary Table S3). In the case of the obtained data from the colorimetric substrate (Suc-VPF-pNA), camostat partly inhibits CatG activity only at high concentrations (500 to 1000 μ M), which might be due to the fact that camostat can bind to the catalytic center of CatG (-6.52 kcal/mol, Figure 3A). This is not the case in the activity-based protein profiling, where camostat has to compete with the ABP, MARS116-FAM, which is a component based on the chemical moiety of SucVPF [23] (-8.75 kcal/mol, Supplementary Table S3).

Besides camostat, various other promising compounds have been used in clinical studies to treat COVID-19, including heparin. For instance, Buijssers et al. showed that administering heparin to COVID-19 patients is beneficial. Heparin might reduce endothelial leakage by inhibiting heparinase, which prevents leukocyte infiltration and promotes anti-coagulation via binding to anti-thrombin III [30]. Remarkably, heparin interacts with CatG in an allosteric manner, provoking a non-competitive inhibition of CatG [31]. Interestingly, another study revealed a concentration-dependent effect of heparin on CatG activity that was significantly diminished by 0.29 μ M heparin, whereas an increase in heparin concentration slightly reversed this effect [32]. We found that an excess of heparin slightly increased the proteolytic activity of CatG [33]. In particular, further investigations are warranted with the significant number of COVID-19 patients who did not benefit from heparin treatment [34,35].

Alpha-1 antitrypsin blocks the catalytic activity of NSPs and TMPRSS2. The anti-inflammation, anti-coagulation, and serine protease inhibitory characteristics of alpha-1 antitrypsin, evident in the treatment of alpha-1 antitrypsin deficiency, render it an attractive component for the COVID-19 treatment [36,37]. Whether alpha-1 antitrypsin prevents SARS-CoV-2 replication in the target cell has been challenged. Therapeutically acceptable concentrations were only achieved with the serine protease inhibitor aprotinin but not for alpha-1 antitrypsin [38]. Aprotinin was found to effectively restrict the infection of influenza A by disrupting viral hemagglutinin cleavage. Moreover, aprotinin administered in an aerosolized form led to a two-fold reduction of symptoms in patients with seasonal influenza A and parainfluenza [39]. Yet, the commercial therapeutic use of aprotinin was suspended in 2008 due to serious cardiovascular, renal, and cerebrovascular adverse events [40,41]. High levels of NE were found in blood samples of COVID-19 patients, which exacerbates the disease [42]; sivelestat might be a therapeutic option as recommended by [43]. Another encouraging component is boswellic acid, which inhibits CatG and NE [44,45]. Camostat, on the other hand, does not inhibit the proteolytic activity of CatG, NE, and PR3, supporting the need to verify other protease inhibitors to manage COVID-19.

3. Materials and Methods

3.1. Activity-Based Protein Profiling

Purified CatG from human neutrophils was purchased from BioCentrum, Ltd. (Krakow, Poland). CatG was adjusted to a final concentration of 80 µg/mL and incubated with the activity-based probe FAM-P1,5D-Suc-Val-Pro-Phe^P(OPh)₂ (MARS116-FAM, final concentration 20 µM) [23] in DPBS pH 7.4 (no calcium, no magnesium, Gibco by Thermo Fisher Scientific, Karlsruhe, Germany, Cat. No.: 14190-094) for 1 h at RT. Samples, including the inhibitors, were preincubated (15 min at RT) with different concentrations of camostat (camostat mesylate, Cayman Chemical Company, Ann Arbor, MI, USA, cat. no.: 16018, batch 0588008-2), 10 µM of CatG inhibitor (CatGinh, Calbiochem, Merck Chemicals GmbH, Schwabach, Germany, CAT. NO.: 219372), or 10 µM of Suc-Val-Pro-Phe^P(OPh)₂ (SucVPF) [19]. All three inhibitors were dissolved in DMSO (Sigma-Aldrich, Taufkirchen, Germany). Afterwards, the samples were reduced, boiled, and resolved by 12% SDS-PAGE (1 µg of CatG per well). CatG activity was visualized by UV light and the Fusion FX6 Edge software (Fusion FX, Vilber Smart Imaging, Eberhardzell, Germany).

Purified NE adjusted to a final concentration of 40 µg/mL (Cat. No. 16-14-051200, lot no. EH2020-03 from Athens Research and Technology, Athens, GA, USA or cat. no. ab280938; lot no. GR3427395-6 from Abcam, Cambridge, MA, USA) or 40 µg/mL PR3 (cat. no. 16-14-161820-L, lot no. PR32020-01, Athens Research and Technology, Athens, GA, USA) were preincubated with different concentrations of camostat (SigmaAldrich, cat. no. SML0057, batch 0000099204) or 10 µM sivelestat (Tocris Bioscience, Bristol, UK, cat. no.: 3535, batch 3A/247536) at room temperature for 15 min. Afterwards, the activity-based probe FAM-DAPe-Suc-Val-Pro-Val^P(OPh)₂ (VPV-FAM, final concentration 10 µM) was added to all samples. The samples were separated by 12% SDS-PAGE and visualized with ChemiDoc Touch Imaging System (Bio-Rad Laboratories, Inc., Hercules, CA, USA).

3.2. Turnover of the Colorimetric Substrate

The turnover of the colorimetric substrate 4-(((S)-3-methyl-1-((S)-2-(((S)-1-((4-nitrophenyl) amino)-1-oxo-3-phenyl-propan-2-yl)-carbamoyl)-pyrrolidin-1-yl)-1-oxobutan-2-yl)-amino)-4-oxobutanoic acid (Suc-VPF-pNA) was determined with CatG (BioCentrum Ltd., Krakow, Poland). A total of 4 µg/mL CatG, 4 µg/mL CatG with 10 µM SucVPF, or CatG with camostat. DMSO (Sigma-Aldrich, Taufkirchen, Germany) was used as the vehicle control. The reagents were preincubated in DPBS pH 7.4 (no calcium, no magnesium, Gibco by Thermo Fisher Scientific, Karlsruhe, Germany, cat. no.: 14190-094) for 15 min at RT previous addition of the colorimetric substrate Suc-VPF-pNA (final concentration 200 µM). The samples were measured in a 96-well plate reader (Spectra Max 250, MWG Biotech, Ebersbach, Germany) at 405 nm.

3.3. Molecular Docking

CatG (1CGH) and Tmprss2 (7MEQ), NE (1B0F), and PR3 (1FUJ) were retrieved from the Protein Data Bank (PDB). AutoDock Tools (ADT) was used to remove heteroatoms, add polar hydrogens, compute Kollman and Gasteiger charges, and generate PDBQT formatted files. The ligand structures for camostat, GBA, CatG inhibitor, and sivelestat were obtained from PubChem in SMILES formats. SucVPF was downloaded from the BRENDA database in mol format (Supplementary Table S1). The ligands were prepared using ADT and optimized using the MMFF94 mechanical force field implemented in the Avogadro program and converted into PDBQT format using OpenBabel.

AutoDock4 version (4.2.6) for macOS X (Scripps Research, AutoDock, retrieved from <https://autodock.scripps.edu/download-autodock4/>, accessed on 3 June 2020) was applied to one ligand (flexible) and one protein (rigid) at a time using the Lamarckian genetic algorithm with extended search parameters GA-run 50 and ga_pop_size 300 limited to 50 poses. The ability of AutoDock4 to reproduce the position of co-crystallized ligands contained in each PDB structure was validated by redocking CatG and SucVPF (1CGH), Tmprss2 and GBA (7MEQ) (Figure 3, Supplementary data Table S2) as well as NE

(Figure 4, Supplementary data Table S3) and PR3 (Figure 5, Supplementary data Table S3). The comparison of the redocked compounds with the co-crystallized ligands showed an RMSD of less than 1.5 Å.

Docking for all proteases was performed at the reported binding sites by adopting a grid size of $40 \times 40 \times 40$ Å along the three axes and a grid point spacing of 0.5 Å. Fifty conformations were generated with AutoDock4. Models with the lowest free binding energy were ranked first upon clustering of similar poses with an RMSD threshold of 2 Å and were used as representative poses shown in the figures. Overall, the best binding conformations for the inhibitors possess the lowest binding free energies and molecular interactions with pivotal amino acid residues. Protein–ligand interactions were visualized and analyzed using PLIP and PyMol. Potential molecular interactions between the compounds and the active-site amino acid residues of proteases, along with the free binding energies and K_i , are shown in Supplementary Tables S2 and S3. Software and online tools used for molecular docking procedures are listed in Supplementary Table S4.

3.4. Statistical Analysis

Bar diagrams, including mean with standard deviation (SD) and p -value (<0.01) threshold, were generated with Graph Pad Prism (GraphPad Prism 8 for macOS, Version 8.4.3, 471, GraphPad Software, Inc., San Diego, CA, USA). A one-way ANOVA for multiple comparisons of CatG, DMSO, SucVPF, and camostat (Figure 1C) or unpaired, two-tailed Student's t -test (no inhibitor, DMSO) versus camostat (Figure 1D), was applied.

4. Conclusions

The proteolytic activity of proteases needs to be tightly regulated to avoid harmful consequences. In such conditions, Figure 6 exemplifies the synergy between CatG and inflammation resulting in cardiovascular diseases, including thrombosis, and the possible therapeutic approach for treating COVID-19 patients.

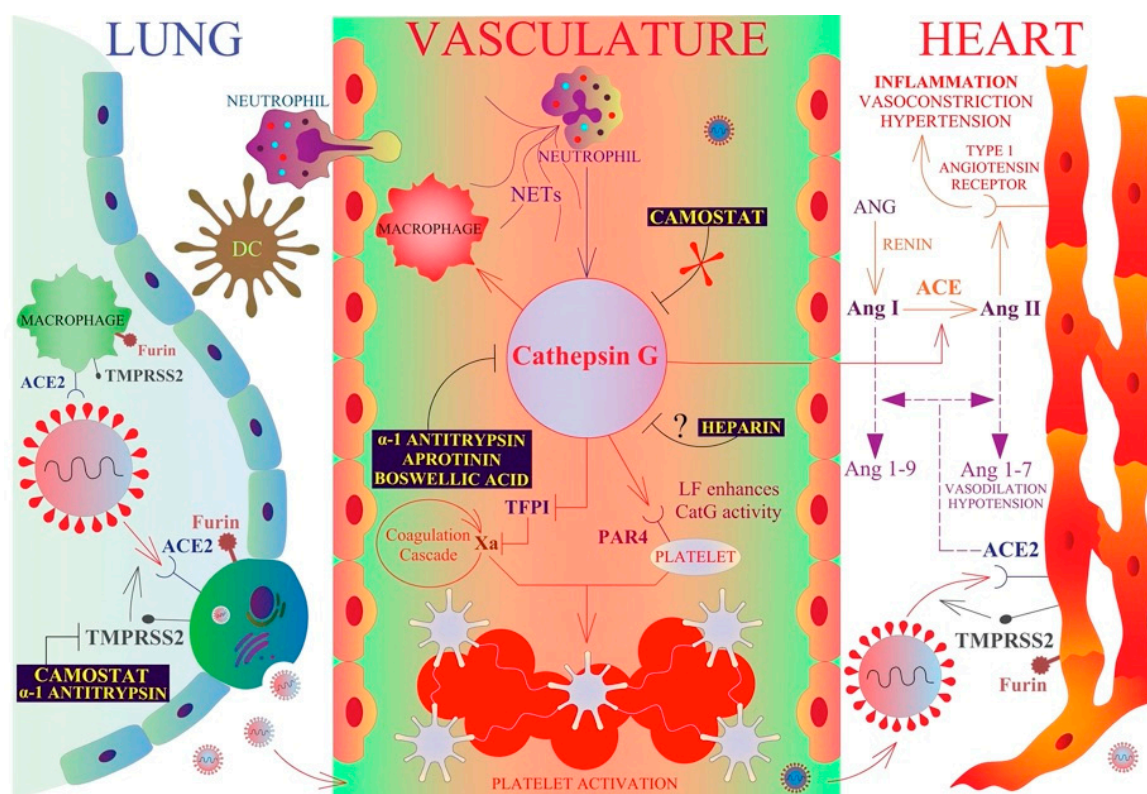


Figure 6. A model of CatG in SARS-CoV-2 infection and inflammation. Activated neutrophils segregate CatG into extracellular space where CatG hydrolyzes the protease-activated receptor 4 (PAR4) on the

surface of platelets, which can cause platelet aggregation, coagulation, and thrombosis formation in the vasculature. Thereby, lactoferrin (LF) enhances CatG-mediated platelet activation. Additionally, CatG promotes the recruitment of macrophages and neutrophils to the sites of inflammation and converts angiotensin I (Ang I) to angiotensin II (Ang II) facilitating inflammation, vasoconstriction, and hypertension. Aprotinin, alpha-1 antitrypsin, and boswellic acids are potent inhibitors of CatG, heparin might block CatG activity but in a dose-dependent manner. However, camostat does not inhibit CatG activity (Figure 1). SARS-CoV-2 binds to the ACE2 receptor on type II pneumocytes (lung), alveolar macrophages (lung), and cardiomyocytes (heart), whereas furin and TMPRSS2 prime the SARS-CoV-2-S protein for viral entry into the host cell. Camostat and alpha-1 antitrypsin are potent inhibitors of TMRPSS2 and interfere with productive infection by SARS-CoV-2. ACE2 can convert Ang I and Ang II to Ang 1–9 and Ang 1–7, respectively [11,46].

Supplementary Materials: The following supporting information can be downloaded at: <https://www.mdpi.com/article/10.3390/ph15050500/s1>, Table S1: Ligand information; Table S2: Amino acids involved in protein–ligand interactions for docking TMPRSS2 and CatG; Table S3: Amino acids involved in protein–ligand interactions for docking of NE and PR; Table S4: Software and online tools used.

Author Contributions: Conceptualization, T.B.; methodology, A.A. and C.S.; software, A.A. and C.S.; validation, T.B. and C.S.; formal analysis, T.B., A.A., C.S. and R.G.; investigation, A.A., R.G. and T.B.; resources, M.S. and R.G.; writing—original draft preparation, T.B. and A.A.; writing—review and editing, A.A., T.B., C.S., R.G., M.S. and A.Z.; visualization, A.Z.; supervision, T.B.; project administration, T.B.; funding acquisition, T.B. All authors have read and agreed to the published version of the manuscript.

Funding: This research was funded by the Nazarbayev University Faculty-Development Competitive research grant program, reference: 280720FD1907.

Institutional Review Board Statement: Not applicable.

Informed Consent Statement: Not applicable.

Data Availability Statement: Data is contained within the article and supplementary material.

Acknowledgments: We appreciate the support from Reinhold Schirmbeck (University Hospital Ulm, Internal Medicine I, Ulm, Germany) for the camostat and help with the CatG assay.

Conflicts of Interest: The authors declare no conflict of interest.

References

1. Belouzard, S.; Chu, V.C.; Whittaker, G.R. Activation of the SARS coronavirus spike protein via sequential proteolytic cleavage at two distinct sites. *Proc. Natl. Acad. Sci. USA* **2009**, *106*, 5871–5876. [[CrossRef](#)] [[PubMed](#)]
2. Millet, J.K.; Whittaker, G.R. Host cell entry of Middle East respiratory syndrome coronavirus after two-step, furin-mediated activation of the spike protein. *Proc. Natl. Acad. Sci. USA* **2014**, *111*, 15214–15219. [[CrossRef](#)] [[PubMed](#)]
3. Matsuyama, S.; Nagata, N.; Shirato, K.; Kawase, M.; Takeda, M.; Taguchi, F. Efficient activation of the severe acute respiratory syndrome coronavirus spike protein by the transmembrane protease TMPRSS2. *J. Virol.* **2010**, *84*, 12658–12664. [[CrossRef](#)] [[PubMed](#)]
4. Bertram, S.; Dijkman, R.; Habjan, M.; Heurich, A.; Gierer, S.; Glowacka, I.; Welsch, K.; Winkler, M.; Schneider, H.; Hofmann-Winkler, H.; et al. TMPRSS2 activates the human coronavirus 229E for cathepsin-independent host cell entry and is expressed in viral target cells in the respiratory epithelium. *J. Virol.* **2013**, *87*, 6150–6160. [[CrossRef](#)] [[PubMed](#)]
5. Bestle, D.; Heindl, M.R.; Limburg, H.; Van Lam, T.; Pilgram, O.; Moulton, H.; Stein, D.A.; Hards, K.; Eickmann, M.; Dolnik, O.; et al. TMPRSS2 and furin are both essential for proteolytic activation of SARS-CoV-2 in human airway cells. *Life Sci. Alliance* **2020**, *3*. [[CrossRef](#)] [[PubMed](#)]
6. Sakr, Y.; Bensasi, H.; Taha, A.; Bauer, M.; Ismail, K. Camostat mesylate therapy in critically ill patients with COVID-19 pneumonia. *Intensive Care Med.* **2021**, *47*, 707–709. [[CrossRef](#)]
7. Talukdar, R.; Saikia, N.; Singal, D.K.; Tandon, R. Chronic pancreatitis: Evolving paradigms. *Pancreatology* **2006**, *6*, 440–449. [[CrossRef](#)]
8. Kahler, J.P.; Vanhoutte, R.; Verhelst, S.H.L. Activity-Based Protein Profiling of Serine Proteases in Immune Cells. *Arch. Immunol. Ther. Exp.* **2020**, *68*, 23. [[CrossRef](#)]

9. Burgener, S.S.; Leborgne, N.G.F.; Snipas, S.J.; Salvesen, G.S.; Bird, P.I.; Benarafa, C. Cathepsin G Inhibition by Serpinb1 and Serpinb6 Prevents Programmed Necrosis in Neutrophils and Monocytes and Reduces GSDMD-Driven Inflammation. *Cell Rep.* **2019**, *27*, 3646–3656.e5. [[CrossRef](#)]
10. Burster, T.; Knippschild, U.; Molnar, F.; Zhanapiya, A. Cathepsin G and its Dichotomous Role in Modulating Levels of MHC Class I Molecules. *Arch. Immunol. Ther. Exp.* **2020**, *68*, 25. [[CrossRef](#)]
11. Burster, T.; Mustafa, Z.; Myrzakhmetova, D.; Zhanapiya, A.; Zimecki, M. Hindrance of the Proteolytic Activity of Neutrophil-Derived Serine Proteases by Serine Protease Inhibitors as a Management of Cardiovascular Diseases and Chronic Inflammation. *Front. Chem.* **2021**, *9*, 784003. [[CrossRef](#)] [[PubMed](#)]
12. Wargodsky, R.; Dela Cruz, P.; LaFleur, J.; Yamane, D.; Kim, J.S.; Benjenk, I.; Heinz, E.; Irondi, O.O.; Farrar, K.; Toma, I.; et al. RNA Sequencing in COVID-19 patients identifies neutrophil activation biomarkers as a promising diagnostic platform for infections. *PLoS ONE* **2022**, *17*, e0261679. [[CrossRef](#)] [[PubMed](#)]
13. Akgun, E.; Tuzuner, M.B.; Sahin, B.; Kilercik, M.; Kulah, C.; Cakiroglu, H.N.; Serteser, M.; Unsal, I.; Baykal, A.T. Proteins associated with neutrophil degranulation are upregulated in nasopharyngeal swabs from SARS-CoV-2 patients. *PLoS ONE* **2020**, *15*, e0240012. [[CrossRef](#)] [[PubMed](#)]
14. Beloglazov, V.; Yatskov, I.; Nikolaeva, A.; Lavrenchuk, E.; DuBuske, L. Cathepsin G in Patients with SARS-Cov-2 Infection of Various Degrees of Severity. *J. Allergy Clin. Immunol.* **2022**, *149*, AB59. [[CrossRef](#)]
15. Mustafa, Z.; Kalbacher, K.; Burster, T. Occurrence of a novel cleavage site for cathepsin G adjacent to the polybasic sequence within the proteolytically sensitive activation loop of the SARS-CoV-2 Omicron variant: The amino acid substitution N679K and P681H of the spike protein. *PLoS ONE* **2022**, *17*, e0264723. [[CrossRef](#)]
16. Kosikowska, P.; Lesner, A. Inhibitors of cathepsin G: A patent review (2005 to present). *Expert Opin. Ther. Pat.* **2013**, *23*, 1611–1624. [[CrossRef](#)]
17. Legowska, A.; Debowski, D.; Lesner, A.; Wysocka, M.; Rolka, K. Introduction of non-natural amino acid residues into the substrate-specific P1 position of trypsin inhibitor SFTI-1 yields potent chymotrypsin and cathepsin G inhibitors. *Bioorg. Med. Chem.* **2009**, *17*, 3302–3307. [[CrossRef](#)]
18. Swedberg, J.E.; Li, C.Y.; de Veer, S.J.; Wang, C.K.; Craik, D.J. Design of Potent and Selective Cathepsin G Inhibitors Based on the Sunflower Trypsin Inhibitor-1 Scaffold. *J. Med. Chem.* **2017**, *60*, 658–667. [[CrossRef](#)]
19. Oleksyszyn, J.; Powers, J.C. Irreversible inhibition of serine proteases by peptide derivatives of (alpha-aminoalkyl)phosphonate diphenyl esters. *Biochemistry* **1991**, *30*, 485–493. [[CrossRef](#)]
20. Kawabata, K.; Suzuki, M.; Sugitani, M.; Imaki, K.; Toda, M.; Miyamoto, T. ONO-5046, a novel inhibitor of human neutrophil elastase. *Biochem. Biophys. Res. Commun.* **1991**, *177*, 814–820. [[CrossRef](#)]
21. Aikawa, N.; Kawasaki, Y. Clinical utility of the neutrophil elastase inhibitor sivelestat for the treatment of acute respiratory distress syndrome. *Ther. Clin. Risk Manag.* **2014**, *10*, 621–629. [[CrossRef](#)] [[PubMed](#)]
22. Hwang, T.L.; Wang, W.H.; Wang, T.Y.; Yu, H.P.; Hsieh, P.W. Synthesis and pharmacological characterization of 2-aminobenzaldehyde oxime analogs as dual inhibitors of neutrophil elastase and proteinase 3. *Bioorg. Med. Chem.* **2015**, *23*, 1123–1134. [[CrossRef](#)]
23. Schroeder, R.; Grzywa, R.; Wirtz, C.R.; Sienczyk, M.; Burster, T. Application of a novel FAM-conjugated activity-based probe to determine cathepsin G activity intracellularly. *Anal. Biochem.* **2020**, *588*, 113488. [[CrossRef](#)] [[PubMed](#)]
24. Burster, T.; Gartner, F.; Knippschild, U.; Zhanapiya, A. Activity-Based Probes to Utilize the Proteolytic Activity of Cathepsin G in Biological Samples. *Front. Chem.* **2021**, *9*, 628295. [[CrossRef](#)]
25. Hoffmann, M.; Kleine-Weber, H.; Schroeder, S.; Kruger, N.; Herrler, T.; Erichsen, S.; Schiergens, T.S.; Herrler, G.; Wu, N.H.; Nitsche, A.; et al. SARS-CoV-2 Cell Entry Depends on ACE2 and TMPRSS2 and Is Blocked by a Clinically Proven Protease Inhibitor. *Cell* **2020**, *181*, 271–280. [[CrossRef](#)]
26. Gunst, J.D.; Staerke, N.B.; Pahus, M.H.; Kristensen, L.H.; Bodilsen, J.; Lohse, N.; Dalgaard, L.S.; Bronnum, D.; Frobert, O.; Honge, B.; et al. Efficacy of the TMPRSS2 inhibitor camostat mesilate in patients hospitalized with COVID-19—a double-blind randomized controlled trial. *eClinicalMedicine* **2021**, *35*, 100849. [[CrossRef](#)] [[PubMed](#)]
27. Zhu, H.; Du, W.; Song, M.; Liu, Q.; Herrmann, A.; Huang, Q. Spontaneous binding of potential COVID-19 drugs (Camostat and Nafamostat) to human serine protease TMPRSS2. *Comput. Struct. Biotechnol. J.* **2021**, *19*, 467–476. [[CrossRef](#)] [[PubMed](#)]
28. Fraser, B.J.; Beldar, S.; Seitova, A.; Hutchinson, A.; Mannar, D.; Li, Y.; Kwon, D.; Tan, R.; Wilson, R.P.; Leopold, K.; et al. Structure, activity and inhibition of human TMPRSS2, a protease implicated in SARS-CoV-2 activation. *bioRxiv* **2021**. [[CrossRef](#)]
29. Hempel, T.; Raich, L.; Olsson, S.; Azouz, N.P.; Klingler, A.M.; Hoffmann, M.; Pohlmann, S.; Rothenberg, M.E.; Noe, F. Molecular mechanism of inhibiting the SARS-CoV-2 cell entry facilitator TMPRSS2 with camostat and nafamostat. *Chem. Sci.* **2021**, *12*, 983–992. [[CrossRef](#)]
30. Buijssers, B.; Yanginlar, C.; Maciej-Hulme, M.L.; de Mast, Q.; van der Vlag, J. Beneficial non-anticoagulant mechanisms underlying heparin treatment of COVID-19 patients. *eBioMedicine* **2020**, *59*, 102969. [[CrossRef](#)]
31. Sissi, C.; Lucatello, L.; Naggi, A.; Torri, G.; Palumbo, M. Interactions of low-molecular-weight semi-synthetic sulfated heparins with human leukocyte elastase and human Cathepsin G. *Biochem. Pharmacol.* **2006**, *71*, 287–293. [[CrossRef](#)] [[PubMed](#)]
32. Fleddermann, J.; Pichert, A.; Arnhold, J. Interaction of serine proteases from polymorphonuclear leucocytes with the cell surface and heparin. *Inflammation* **2012**, *35*, 81–88. [[CrossRef](#)] [[PubMed](#)]

33. Eipper, S.; Steiner, R.; Lesner, A.; Sienczyk, M.; Palesch, D.; Halatsch, M.E.; Zaczynska, E.; Heim, C.; Hartmann, M.D.; Zimecki, M.; et al. Lactoferrin Is an Allosteric Enhancer of the Proteolytic Activity of Cathepsin G. *PLoS ONE* **2016**, *11*, e0151509. [[CrossRef](#)] [[PubMed](#)]
34. Thomas, W.; White, D.; Cox-Morton, S.; MacDonald, S.; Besser, M. Heparin failure and COVID-19: Should we explore other anticoagulants? An observational report regarding in-vitro recovery of anticoagulant action in COVID-19 patients in intensive care. *Thromb. Res.* **2020**, *195*, 226–227. [[CrossRef](#)]
35. Daughety, M.M.; Morgan, A.; Frost, E.; Kao, C.; Hwang, J.; Tobin, R.; Patel, B.; Fuller, M.; Welsby, I.; Ortel, T.L. COVID-19 associated coagulopathy: Thrombosis, hemorrhage and mortality rates with an escalated-dose thromboprophylaxis strategy. *Thromb. Res.* **2020**, *196*, 483–485. [[CrossRef](#)] [[PubMed](#)]
36. Yang, C.; Keshavjee, S.; Liu, M. Alpha-1 Antitrypsin for COVID-19 Treatment: Dual Role in Antiviral Infection and Anti-Inflammation. *Front. Pharmacol.* **2020**, *11*, 615398. [[CrossRef](#)]
37. de Loyola, M.B.; Dos Reis, T.T.A.; de Oliveira, G.; da Fonseca Palmeira, J.; Arganaraz, G.A.; Arganaraz, E.R. Alpha-1-antitrypsin: A possible host protective factor against COVID-19. *Rev. Med. Virol.* **2020**, *31*, e2157. [[CrossRef](#)]
38. Bojkova, D.; Bechtel, M.; McLaughlin, K.M.; McGreig, J.E.; Klann, K.; Bellinghausen, C.; Rohde, G.; Jonigk, D.; Braubach, P.; Ciesek, S.; et al. Aprotinin Inhibits SARS-CoV-2 Replication. *Cells* **2020**, *9*, 2377. [[CrossRef](#)]
39. Zhirnov, O.P.; Klenk, H.D.; Wright, P.F. Aprotinin and similar protease inhibitors as drugs against influenza. *Antivir. Res.* **2011**, *92*, 27–36. [[CrossRef](#)]
40. Lien, M.; Milbrandt, E.B. A disheartening story: Aprotinin in cardiac surgery. *Crit. Care* **2006**, *10*, 317. [[CrossRef](#)]
41. Mangano, D.T.; Miao, Y.; Vuylsteke, A.; Tudor, I.C.; Juneja, R.; Filipescu, D.; Hoeft, A.; Fontes, M.L.; Hillel, Z.; Ott, E.; et al. Mortality associated with aprotinin during 5 years following coronary artery bypass graft surgery. *JAMA* **2007**, *297*, 471–479. [[CrossRef](#)] [[PubMed](#)]
42. Gueant, J.L.; Gueant-Rodriguez, R.M.; Fromonot, J.; Oussalah, A.; Louis, H.; Chery, C.; Gette, M.; Gleye, S.; Callet, J.; Raso, J.; et al. Elastase and exacerbation of neutrophil innate immunity are involved in multi-visceral manifestations of COVID-19. *Allergy* **2021**, *76*, 1846–1858. [[CrossRef](#)] [[PubMed](#)]
43. Sahebnaasagh, A.; Saghafi, F.; Safdari, M.; Khataminia, M.; Sadremomtaz, A.; Talaei, Z.; Ghaleno, H.R.; Bagheri, M.; Habtemariam, S.; Avan, R. Neutrophil elastase inhibitor (sivelestat) may be a promising therapeutic option for management of acute lung injury/acute respiratory distress syndrome or disseminated intravascular coagulation in COVID-19. *J. Clin. Pharm. Ther.* **2020**, *45*, 1515–1519. [[CrossRef](#)] [[PubMed](#)]
44. Safayhi, H.; Rall, B.; Sailer, E.R.; Ammon, H.P. Inhibition by boswellic acids of human leukocyte elastase. *J. Pharmacol. Exp. Ther.* **1997**, *281*, 460–463. [[PubMed](#)]
45. Tausch, L.; Henkel, A.; Siemoneit, U.; Poeckel, D.; Kather, N.; Franke, L.; Hofmann, B.; Schneider, G.; Angioni, C.; Geisslinger, G.; et al. Identification of human cathepsin G as a functional target of boswellic acids from the anti-inflammatory remedy frankincense. *J. Immunol.* **2009**, *183*, 3433–3442. [[CrossRef](#)]
46. Zhang, Q.; Xiang, R.; Huo, S.; Zhou, Y.; Jiang, S.; Wang, Q.; Yu, F. Molecular mechanism of interaction between SARS-CoV-2 and host cells and interventional therapy. *Signal Transduct. Target. Ther.* **2021**, *6*, 233. [[CrossRef](#)]